Experiments in Fluids 28 (2000) 21–28 © Springer-Verlag 2000

# Pressure-sensitive paint measurements in a shock tube

**J. P. Hubner, B. F. Carroll, K. S. Schanze, H. F. Ji**



**Abstract** Surface pressures were measured in the short-duration, transient flow environment of a small-scale, low pressure-ratio shock tube using thin-film pressure-sensitive paint (PSP). Issues regarding coating formulation, measurement uncertainty, optical system design, and temperature and illumination compensation are discussed. The pressure measurements were acquired during steady flow conditions following the passage of normal shocks and expansion regions along a flat sidewall and a wedge sidewall. The PSP characteristic response time was 3 to 6 ms. Overall pressure uncertainty for the shock tube measurements ranged up to 5% over one atmosphere and compared well with theoretical estimates of uncertainty.

**List of symbols**

| | |
|---|---|
| $A$, $B$, $C$, $D$ | PSP coating sensitivities |
| $c$ | wedge characteristic length |
| $C_p$ | pressure coefficient |
| $D_m$ | mass diffusivity |
| $h$ | PSP thickness |
| $I$ | intensity |
| $K$ | Stern–Volmer constant |
| $n$ | number of pixels or images |
| $P$ | pressure |
| $R$ | reflection intensity due to spectral leakage |
| $T$ | temperature |
| $W$ | uncertainty |
| $x$ | streamwise direction |
| $\tau$ | PSP response time |

**Subscripts**

| | |
|---|---|
| $o$ | unquenched ($P=0$) |
| 1, 2, 4 | shock tube state on low pressure side, aft of the initial shock, and high pressure side, respectively |
| ratio | shock tube prerun pressure ratio, $P_4/P_1$ |
| ref | reference condition |

*Received*: *20 April 1998 / Accepted*: *9 September 1998*

J. P. Hubner, B. F. Carroll
Department of Aerospace Engineering, Mechanics, and Engineering Science, PO Box 116250, University of Florida, Gainesville, FL 32611-6250, USA

K. S. Schanze, H. F. Ji
Department of Chemistry, PO Box 117200, University of Florida, Gainesville, FL 32611-7200, USA

*Correspondence to*: J. P. Hubner

The authors would like to thank Andy Winslow for the PSP system identification calculations.

## 1 Introduction

Typical PSPs used in conventional steady-state wind tunnel tests are roughly 20–30 μm thick and have response times on the order of 1 s (Winslow et al. 1996; Carroll et al. 1996). The use of such PSPs has been widely demonstrated in steady flow conditions (Morris et al. 1993; McLachlan and Bell 1995; Lui et al. 1997) where more emphasis is placed on signal strength to increase measurement accuracy, hence the relatively thick coatings. The trade-off is the limited temporal response due to the mass diffusion rate of oxygen within the PSP binder. In order to measure surface pressures under transient or unsteady flow conditions, different approaches are necessary, including but not limited to developing PSPs with high mass diffusivity binders (Baron et al. 1993) and high luminophor concentration near the coating/air interface (Carroll et al. 1996). A more direct approach (Borovoy, 1995; Winslow et al. 1996; Carroll et al. 1996) exploits the relationship between the coating thickness and the characteristic response time:

$$\tau \propto \frac{h^2}{D_m} \tag{1}$$

By using thin coatings ($\sim$2 μm), Borovoy et al. (1995) were able to acquire surface measurements on the lower windward side of a cylinder (30 mm $\varnothing$) in short-duration supersonic flow ($M=6$ and flow duration = 40 ms). Stagnation pressure measurements compared within 10% to conventional pressure gauge measurements.

This paper presents the results and analysis of PSP measurements in a short-duration facility using the principle of thin coatings for fast response. Emphasis was placed on developing the foundation of a PSP measurement system adequate for larger shock tube testing facilities.

## 2 PSP issues

### 2.1 PSP formulation

For the purposes of the present study, the most important feature is the temporal response of the PSP. The temporal

response is determined by the rate at which equilibrium is established between the gas phase and the PSP layer. The thickness of the PSP active layer and the diffusivity of oxygen in the PSP binder (if one is used) control the rate at which equilibrium is established. Consequently, optimum PSP temporal response is attained by (1) using a binder with high oxygen diffusivity and minimizing the thickness of the PSP film or (2) eliminating the binder and placing the luminophor directly at the substrate-gas interface.



Two different PSP binder formulations were assessed to determine the advantages of each in regards to signal strength, measurement sensitivity, and response times. Both formulations used the same luminophor: *tris*-(4,7-diphenylphenanthroline)-Ru(II) dichloride (RudpCl) (Schanze et al. 1997). The RudpCl luminophor was selected for its favorable properties which include a long-luminescence lifetime ($\tau \approx 6$ μs), strong absorptivity in the blue region of the visible spectrum (450 nm optimum), and efficient red luminescence (620 nm maximum). These features allow the PSP to be used as a very thin film, which is a necessary pre-condition for fast temporal response. In the first formulation, the luminophor was dissolved in a polydimethlysiloxane (PDMS) binder using dichloromethane solvent. The solution was applied directly onto the surface of interest using a commercially available airbrush. The temporal response of the PDMS-based PSP was substantially lower when the PSP was applied on top of a white primer (several commercial epoxy- and polyurethane-based primers were tested). The poor temporal response likely arose because the luminophor leached into the primer layer (which has poor oxygen diffusivity) during application of the PSP. Consequently, all experimental work was carried out without a primer layer. In the second formulation (called ESG), the probe molecule was dissolved in methanol and sprayed directly onto a substrate which had been previously coated with a composite film consisting of an epoxy base coat which, prior to curing, had been dip-coated with 5 μm silica gel particles. For both PDMS and ESG formulations, the PSPs, were allowed to cure for over 24 h at ambient temperature. Coating thicknesses, determined via UV absorption, were 4 to 5 μm.

## 2.2 PSP calibration

The steady-state emission response with respect to pressure was tested for the two formulations (PDMS and ESG) at ambient temperature (296 K). Figure 1 shows that when plotted conventionally, a nonlinear Stern–Volmer trend is displayed. The effect is more pronounced for the ESG coating. Explanations for the nonlinear response include the relatively high luminophor loading to binder mass ratio (10 mg Ru/1 g PDMS/10 ml $CH_2Cl_2$) and the microheterogeneous nature of the probe/binder environment. Under such conditions, the luminescent probes can become unevenly dispersed and molecular aggregation can occur, leading to self-quenching of excited probes and multiexponential decays. At low pressure levels, longer decay rates are less likely to be quenched, providing additional luminescence. This is similar to the effect of preferential sorption and penetrent immobilization, which is present in many inhomogeneous polymer films (Vieth et al. 1976; Rogers 1985).

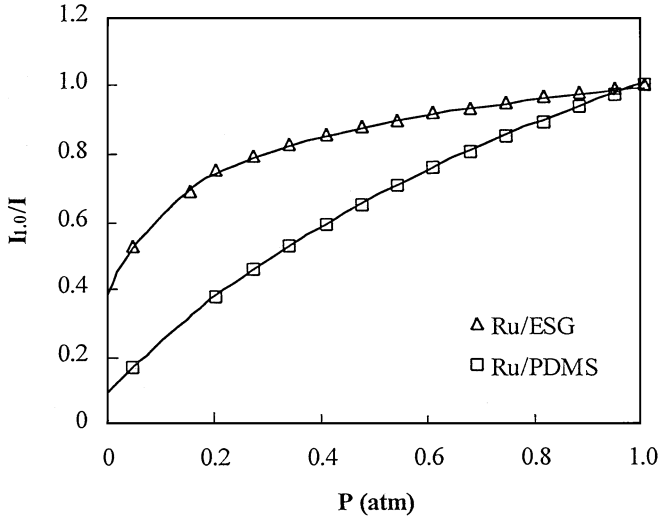


**Fig. 1.** PSP calibration curves

Both sets of PSP data were fit with a dual sorption model equation (Hubner and Carroll 1997), Eq. (2):

$$\frac{I_{\text{ref}}}{I} = A + B\frac{P}{P_{\text{ref}}} + C\frac{D(P/P_{\text{ref}})}{1 + D(P/P_{\text{ref}})} \tag{2}$$

For small pressure ranges near and above atmospheric conditions, the traditional linear model was sufficient, Eq. (3):

$$\frac{I_{\text{ref}}}{I} = A + B\frac{P}{P_{\text{ref}}} \tag{3}$$

The most noticeable difference between the two formulations is the superior sensitivity of the PDMS to the ESG at higher pressures. This is demonstrated by the steeper PDMS curve in Fig. 1. The overall emission intensity, however, was 3 to as much as 10 times larger for the ESG coating. This enhanced emission was partially attributed to the opaque appearance of the coating, assisting in the reflection of the emission (similar to a white primer undercoating). To determine initial dynamic characteristics, the formulations were tested in a calibration rig capable of a 20 ms, one atmosphere pressure rise; both were able to track the pressure rise without a time lag.

## 2.3 Uncertainty analysis

Sajben (1993) and Mendoza (1996) provide good, general assessments of PSP uncertainty. For the purposes of this study, the calculated calibration coefficients of Eq. (2) were used to determine a theoretical uncertainty over a wide range of pressures for both the formulations and the flash/CCD measurement system described in Sect. 3. Three sources of intensity measurement errors were considered: flash repeatability, CCD shot noise, and CCD scene noise. The last error was treated as a systematic bias error and the first two were precision errors. The error values are listed in Table 1. Corrected flash repeatability, using a pressure-insensitive reference strip, was 0.5%. The CCD shot noise was based on the Poisson statistical noise in photon count, and the CCD scene noise was estimated from operator experience with the CCD camera.

**Table 1.** Intensity measurement errors

| Flash | CCD shot noise | CCD scene |
|---|---|---|
| 0.5% of $I$ | $\sqrt{I}$ | 0.5% of $I$ |

**Table 2.** PSP influence coefficients for a single pixel at FWC

| $P$ (atm) | *Ru*/PDMS | *Ru*/ESG |
|---|---|---|
| 0.01 | 0.6 | 0.3 |
| 10 | 5.2 | 10.5 |

The total intensity error was calculated via Eq. (4):

$$W_I = \sqrt{\frac{4W_{\text{Flash}}^2}{n_{\text{images}}} + \frac{4W_{\text{ShN}}^2}{n_{\text{images}} n_{\text{pixels}}} + W_{\text{ScN}}^2} \tag{4}$$

The pressure error was then determined by Eq. (5),

$$W_P = \sqrt{\left(\frac{\partial P}{\partial (I_{\text{ref}}/I)}\, W_{I_{\text{ref}}/I}\right)^2} \tag{5}$$

where $\partial P/\partial(I_{\text{ref}}/I)$ is the influence coefficient determined from the calibration coefficients of Eq. (2) and a full-well capacity (FWC) of $I = 320000$ e$^-$ or (16000 analog-to digital units) at $P = 0$. Pixel binning of $1 \times 1$ and $5 \times 5$ were assumed in the calculations. The results show that the influence coefficient increased at higher pressures, indicating lower pressure sensitivity, for both formulations. Table 2 lists the results for 0.01 and 10 atm.

Figure 2 is a plot of the calculated pressure uncertainty using Eqs. (4) and (5) over a three-decade pressure change for various combinations of pixel binning and FWC. Examination of Fig. 2 shows that if FWC is assumed for both PSPs and similar bin sizes are compared then *Ru*/PDMS has a lower overall uncertainty for most or all of the pressure range. However, for a set integration time, the emission intensity of *Ru*/ESG (for equal luminophor concentration) is larger than the emission intensity of *Ru*/PDMS. Thus, comparing the two PSPs for a set integration time (*Ru*/PDMS at 10% FWC and *Ru*/ESG at 100% FWC) shows that there is a crossover point in terms of bin size ($3 \times 3$ and smaller) were the *Ru*/ESG has a lower pressure uncertainty.

These trends stem from the fact that *Ru*/PDMS has better sensitivity (as seen by the steeper slope in Fig. 1) but lower relative emission strength making it more prone to shot-noise errors when compared to *Ru*/ESG. Due to the high spatial resolution of the CCD and the relatively small pressure-gradient expected in the test environment ( ~0.0005 atm/pixel), pixel binning was affordable; hence, the *Ru*/PDMS formulation was chosen because of its lower uncertainty, good temporal response, and conventional application to the model surface.

## 3 Experimental facility & procedures

### 3.1 Shock tube

The shock tube used in the tests was modular in design allowing variable test section location with respect to the diaphragm and end walls. A schematic of the shock tube is shown in Fig. 3. For all the runs reported in this paper, the test section was located 80+ tube diameters downstream of the diaphragm. The test section cross-sectional area was 918 mm$^2$. Optical access was limited to a $95 \times 16$ mm region. Flat and wedge plates coated with PSP were installed on the side opposite of the optical access. The tube extended another 80 diameters beyond the test section. Prerun pressure levels were set and controlled with vacuum and high pressure lines plumbed into the end sections of the shock tube.

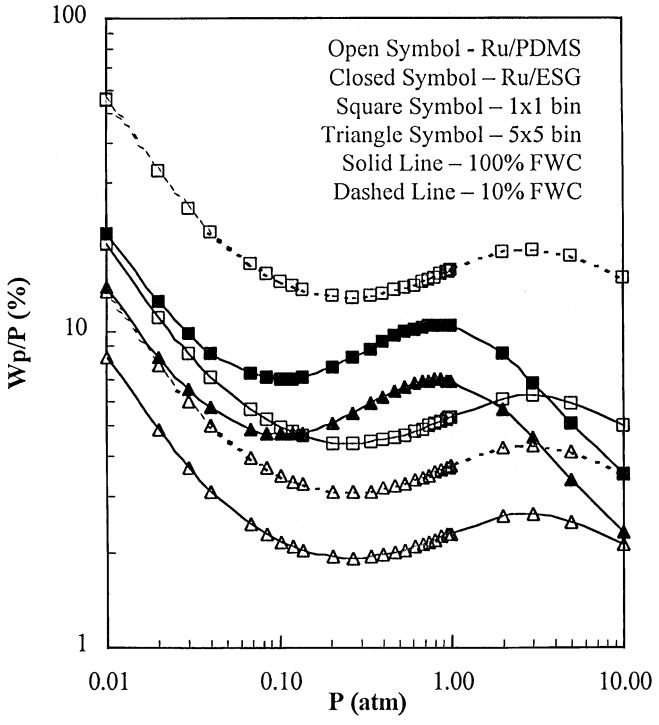


**Fig. 2.** PSP measurement uncertainty

Natural rubber latex film (0.1 and 0.2 mm thick) was used as the diaphragm material. The latex film diaphragm extended into the driven section once the prerun pressure ratio was set. Prestretching the latex film minimized this extension to about one tube diameter. Bursting of the diaphragm was controlled mechanically with a micro pick inserted through a serum cap. Other diaphragm materials were tested such as aluminum foil, polyethylene, high-density polyethylene, and mylar, but all demonstrated irregular or poor bursting characteristics at low pressure ratios.

### 3.2 Instrumentation

#### 3.2.1 Pressure and temperature devices

Test section surface pressure was monitored with a fast-response (1% full-scale accuracy) piezoresistive pressure transducer. This transducer was calibrated prior to each run during the evacuation of the test section. Driver, driven, and trigger signal pressures were monitored with preamplified (1% full-scale accuracy) piezoresistive transducers. The trigger signal was conditioned to generate a step signal that controlled

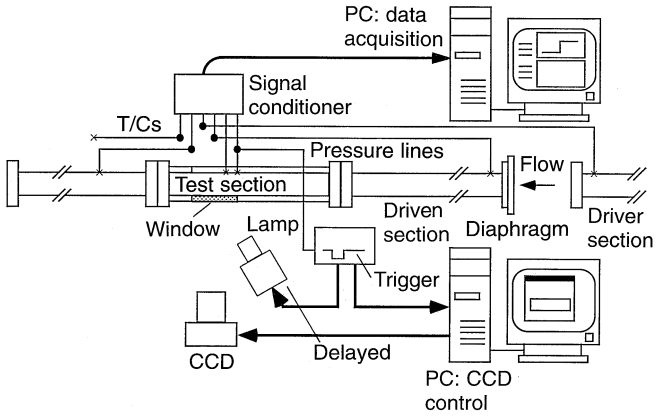


**Fig. 3.** Schematic of shock tube assembly and instrumentation

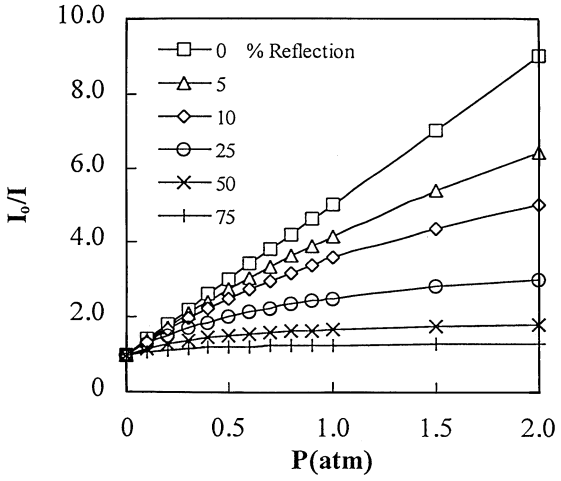


**Fig. 4.** Effect of spectral leakage reflection on a linear Stern–Volmer calibration

the occurrence of the camera shutter and flash events. Two *T*-type thermocouples were used to measure the driver temperatures prior to bursting the diaphragm.

### 3.2.2
### Flash system and optical filters

The PSP coated surfaces were excited with a single UV-corrected Xenon flash tube. Discharge energy to the tube was 50–400 J corresponding to flash durations (99% of total integrated intensity) of 1.2–6.7 ms, respectively. Normalized spatial variance of the flash intensity measured across the CCD pixel field was 0.2% of $5 \times 5$ pixel regions. Overall flash repeatability when corrected using a intensity reference strip was 0.5%.

The peak transmission wavelengths of the excitation and emission interference filters were 450 nm (40 nm full-width-half-maximum: FWHM) and 650 nm (80 nm FWHM), respectively. The filters were 50 mm $\varnothing$. The excitation filter was mounted to a 203 mm $\varnothing$ flash tube reflector. The reflector region uncovered by the excitation filter was blocked with a shield. The emission filter was directly installed behind the lens mount of the CCD camera. Upon filtering with the 450 nm interference filter, about 1% of the original flash intensity was available for PSP excitation. Total emission-filtered intensity of the PSP measured by the CCD was ~1/25000 for the unfiltered flash intensity; thus, emphasizing the need of high-powered excitation sources – especially for large area measurements.

The suitability of gel filters was tested as an alternative to the interference filters. Gel filters offer low cost, large size, high peak transmission, and ease of use. To compare the relative effectiveness of the two filters, the test section sidewall was partially coated with PSP, leaving a bare region, and excited using a gel-filtered (Kodak 47B) and interference filtered (450 nm, 40 FWHM) flash. Ideally, when imaging with an emission filter (650 nm, 80 FWHM), the PSP region would exhibit luminescence and the bare region would be dark. The ratio of the two intensities, referred to as an emission-to-reflection ratio, provides an indication of the excitation filter's effectiveness. The interference filter showed superior isolation of the flash excitation: an emission-to-reflection ratio of ten. The ratio was increased when the distance between the plate and flash/CCD was increased (at the expense of lower intensity measurements). The emission-to-reflection ratio for the gel filter was generally around two and for some worst cases approached one. This is believed to be due to the near infrared transmission of the gel filters. Above 700 nm, most blue gel filters transmit energy which can pass through the tail of emission filters with a broad optimal bandpass, creating a region of crosstalk between the filters.

The effect of measured intensity due to spectral leakage reflections, *R*, is demonstrated in Fig. 4. A simple linear Stern–Volmer emission response ($K=4$) and a constant spectral leakage reflection intensity for varying pressures are assumed, Eq. (6):

$$I=\frac{I_0}{1+KP}+R \tag{6}$$

The results show a substantial decrease in sensitivity due to increasing reflection percentage.

### 3.2.3
### PMT and CCD camera

PSP response times were measured in the shock tube using a photomultiplier tube (PMT) and amplifier unit. The temporal bandwidth of the PMT was 20 kHz. PMT optics collected PSP emission over a region of approximately 100 $mm^2$.

Full-field PSP emission intensities were measured with a thermoelectrically cooled, 14-bit CCD camera. The maximum CCD pixel area was $512 \times 512$. An 8 ms delay was incorporated in the trigger process to account for the shutter opening time.

### 3.3
### Data acquisition and reduction procedures

Surface pressures and temperature measurements were acquired with a personal computer via a 12-bit A/D board. Scan rates were 1 kHz with 4*x* oversampling. Data acquisition and reduction was automated and performed using object-oriented software. The CCD camera was controlled with a separate personal computer. The CCD exposure time was 1 s. Post processing of the images was performed using matrix-oriented software.

## 4
## Results and discussion

### 4.1
### Shock tube flow environment

The shock tube was designed to run with (closed-end) and without (open-end) a driver section. In the latter case, laboratory atmospheric pressure was the driving condition. In all test runs, the initial driver and driven temperatures were equivalent. Under normal run conditions, test section run times were limited by the passing of the reflected shock. Typical time-envelopes were approximately 15 ms with $P_{ratio}$ ranging between 1.2 and 1.5. Initial shock speeds ranged between $M = 1.05$ to 1.2, and temperature increases in the flow ranged between 15 and 25 K behind the reflected shock.

### 4.2
### Flat plate measurements

Initial tests were performed on a flat aluminum plate. Because a pressure-gradient is not present in this configuration, an *in-situ* calibration is not possible. Therefore, the PSP coated plate was calibrated by varying the test section pressure prior to running the shock tube. In most cases, the prerun test section pressure was selected as the reference pressure and image condition. Figure 5 shows a typical calibration of the paint. Over the limited high-pressure range, a linear fit calibration curve was sufficient to model the steady-state response. The PSP pressure error ranged between 2% at 0.5 atm to 4% at 1.2 atm and are based on the approach in Sect. 2.3.

#### 4.2.1
#### PMT results

Figure 6 shows the response of the PSP to the step pressure changes caused by the passage of the initial and reflected shocks. Excitation was supplied from a continuous source and emission intensity was collected over a 100 $mm^2$ region using the PMT. PSP characteristic response times were calculated assuming a first-order system identification algorithm described by Winslow et al. (1996). Characteristic times ranged between 3.5 and 6 ms for similar run conditions. In order to allow the PSP to equilibrate for tests using the flash excitation, a corresponding delay between the passage of the shock and flash was incorporated into the overall timing scheme to account for the PSP response lag.

#### 4.2.2
#### CCD camera results

Full-field measurements were acquired at various instances after the passage of the initial shock by controlling the delay time between the measured pressure trigger and the generated flash trigger. The measurement region was $100 \times 100$ pixels ($15 \times 15$ mm). Run images were ratioed with reference images to correct for varying illumination and coating nonuniformities. Image mapping to account for the possibility of shifting between reference and run images was not necessary.

Results for an open-end test run, $P_{ratio} = 1.47$ and $P_2 = 92.4$ kPa, are displayed in Fig. 7. The flash intensity was set

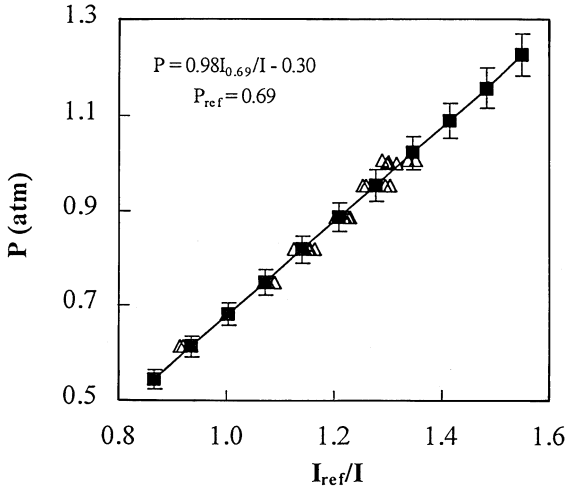


**Fig. 5.** *A priori* PSP calibration over a limited pressure range (linear fit). Square symbols are PSP calibrated data, triangular symbols are PSP raw data

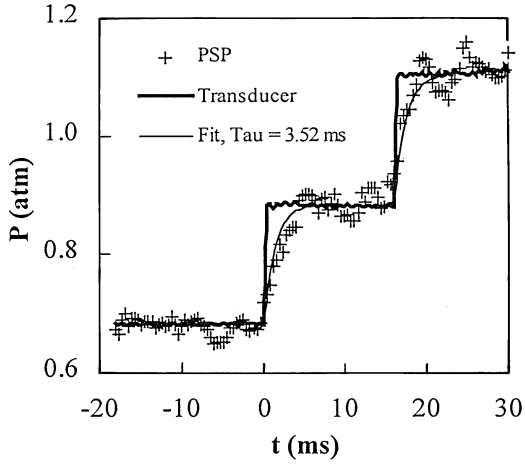


**Fig. 6.** PSP response time to a step change in pressure (passage of initial and reflected normal shocks)

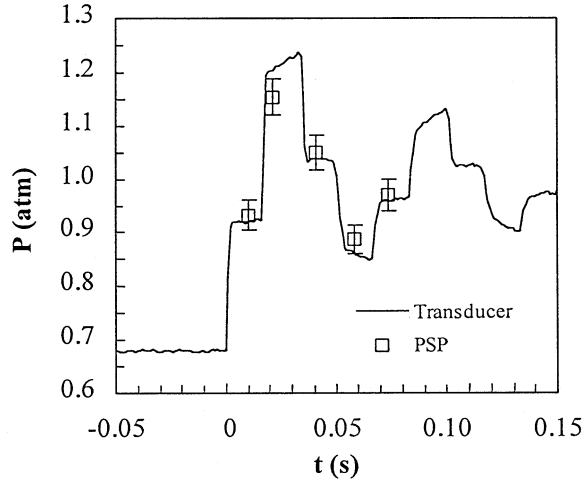


**Fig. 7.** Test section pressure measurement comparison at various times during the pressure trace (five separate test runs for PSP measurements)

at the maximum 400 J, and only 10% of the CCD full-well capacity was utilized. Despite the low intensity readings, four of the five measurements compare well with the conventional pressure transducer. For each measurement instance, the spatial variance of the pressure measurements across the flat-plate was approximately 2% for $5 \times 5$ pixel bins. The poorest measurement occurred after the passage of the reflected shock: 5% below the transducer measurement. This is primarily due to the low signal strength at higher pressures. Additionally, this measurement is the only one that under predicted the actual pressure. The overprediction in pressure by the other four PSP measurements is consistent with an increasing temperature effect behind the initial shock. PSP emission intensity decreases with increasing temperature due to the competition between radiative and nonradiative relaxation processes. Increases in temperature would lower the intensity measured by the CCD, which in turn corresponds to a higher pressure. For the PDMS formulation, the temperature sensitivity is 1.5% /K. If the small pressure over prediction shown in Fig. 7 is due to temperature effects, then this would correspond to a 1–2 K change in the PSP temperature based on the PSP temperature sensitivity. The important detail concerning the PSPs measurements described above is that no temperature correction was applied despite a ~25 K increase in the static temperature behind the initial shock. This is consistent with the results of Borovoy et al. (1995).



A confirmation test with a temperature sensitive paint (TSP) was conducted to further substantiate the minimal PSP temperature effect for the short-duration flow. Based on the thickness of the coating and assuming that the coating thermal diffusivity is determined by the properties of the binder, the effective response time of the coating was calculated to be on the order of 100 μs. The TSP temperature sensitivity is lower than the PSP temperature sensitivity, 0.6% /K, but is insensitive to pressure. While it was not expected that the coating would be able to measure a 1 to 2 K temperature change (the corresponding decrease in intensity of approximately 1% is less than the uncertainty in the measurement), it would indicate if there was a large increase in surface temperature due to the increase in temperature of the flow behind the shock. Intensity ratio results for a test plate coated with both TSP and PSP (no insulating layer or undercoat) is shown in Fig. 8 for two run conditions. The PSP responded to a decrease in pressure (as referenced to atmospheric pressure) for both runs, but the TSP showed no change for either run. The TSP intensity-ratio was essentially unity. A measured increase in temperature compared to the reference condition should lower emission intensity and thus increase the temperature intensity-ratio. However, due to the high thermal conductivity of the aluminum test plate and its large mass with respect to the coating, the plate effectively maintained the temperature of the coating at prerun test conditions.

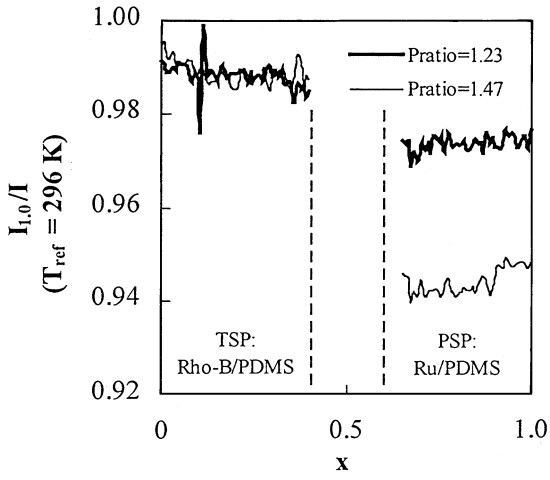


**Fig. 8.** TSP and PSP intensity response to test section flow conditions behind the initial shock: driver open to atmosphere for both runs

## 4.3
## Surface wedge measurements

Surface pressure measurements were next obtained on a wedge fitted to the test section sidewall in order to measure a varying pressure field. The wedge contracted the test section cross-sectional area in half. Fig. 9a is a schematic of the wedge and the imaging area. By decreasing the test section area, the subsonic flow behind the initial shock would increase as the area decreases, forming a decreasing pressure-gradient behind the initial shock and the direction of the flow. Insertion of the wedge into the test section blocked the access of static measurement ports; thus, an *a priori* calibration was used. Fig. 9b is a surface pressure contour plot for a test run of $P_{ratio} = 1.47$ and $P_2 = 92.4$ kPa. Flow direction is from left to right. The contour shows a mild adverse pressure-gradient forming over the leading portion of the wedge. In this region the cross-section area is decreasing; however, the surface width of the wedge is expanding. The net effect is a small pressure increase in the streamwise direction and a mild gradient in the transverse direction. Further downstream along the wedge, a strong favorable gradient is formed, continuing slightly beyond the leveling of the wedge. Beyond the low-pressure region, the pressure increases towards a value predicted by one-dimensional, subsonic flow.

Centerline $C_p$ plots for the shock tube test conditions described above (Shock Run 1) as well as a close-end test run at $P_{ratio} = 1.47$ and $P_2 = 55.2$ kPa (Shock Run 2) are shown in Fig. 10. Because no conventional pressure measurements were available to compare with the PSP measurements, the experimental set-up was reconfigured, and the test section was attached to a continuous high-pressure air supply. The resulting configuration was run continuously, matching the subsonic freestream speed of Run 1. Using a continuous light source enabled the CCD camera to acquire measurements for long durations compared to the flash, hence increasing the PSP signal strength. The $C_p$ results from the continuous run quantitatively compares well with the shock runs. All three PSP measurements show a mild adverse pressure-gradient near the leading-edge and a substantial low pressure "undershoot" at the location where the wedge initially levels off. Theoretical calculations based on one-dimensional, isentropic flow are also plotted for qualitative comparison.

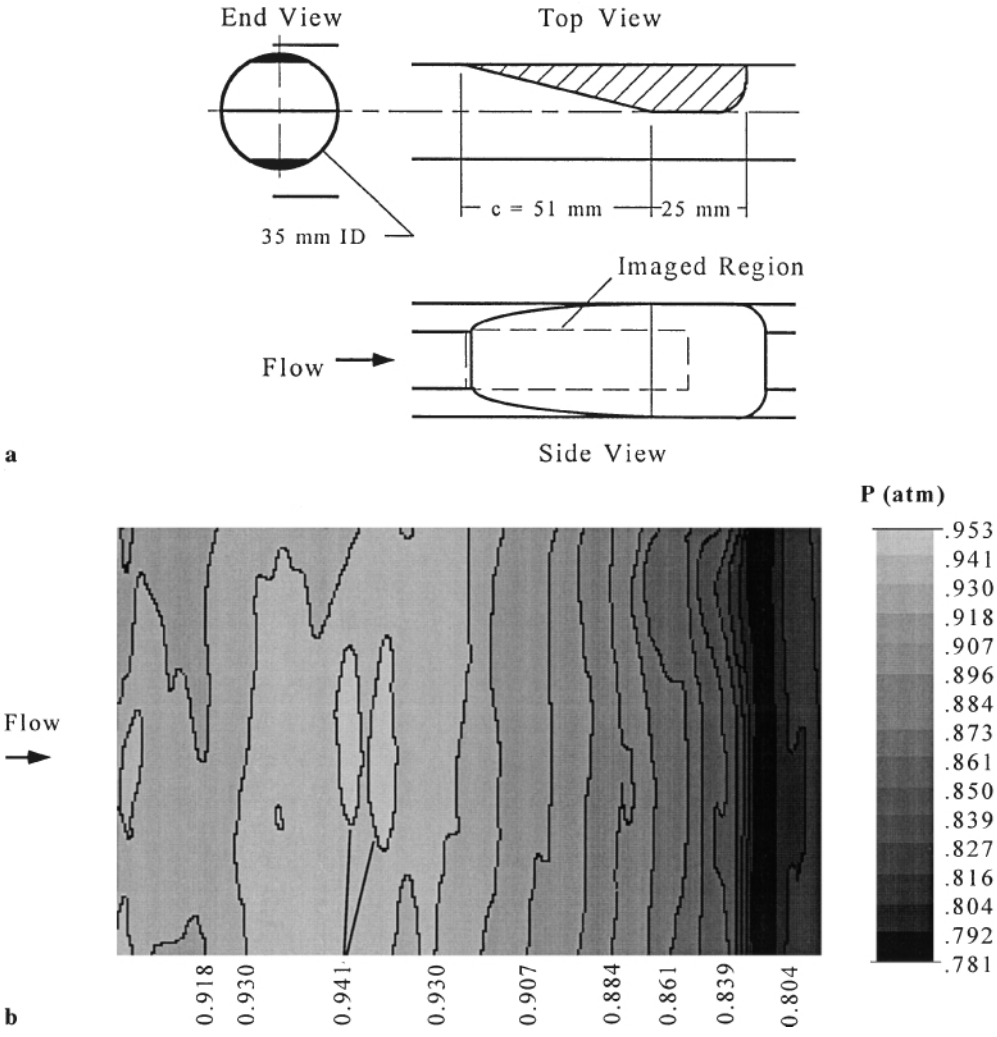


**Fig. 9.** **a** Schematic of wedge insert, **b** wedge surface pressure contour: $P_{ratio} = 1.47$, driver open to atmosphere

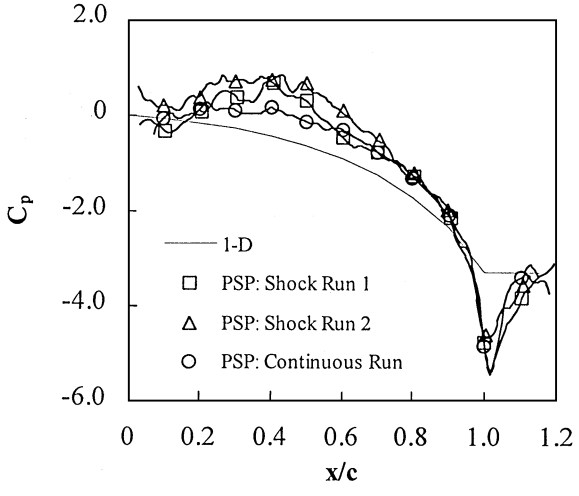


**Fig. 10.** Wedge center line $C_p$ comparison with various runs and 1-D, isentropic theory

## 5 Conclusions

Full-field pressure measurements were successfully obtained in a short-duration, small-scale shock tube. The following conclusions are made:

- Thin-film PSP is a viable technique to measure surface pressures in short-duration facilities. The characteristic response times to step changes in pressure for the coating developed in this paper were 3 to 6 ms (coating thickness of 4–5 μm). Calibration tests demonstrated that the coatings accurately tracked a pressure increase rate of five atmospheres per second over zero to one atmosphere.
- Overall measurement uncertainty for shock tube PSP measurements ranged up to 5%. This error compared well with a theoretical assessment of uncertainty based on excitation repeatability, CCD shot noise, and estimated CCD scene noise.
- Interference filters demonstrated superior rejection characteristics over gel filters. Excitation and emission filter crosstalk using gel filters caused the relative sensitivity of the measured CCD signal to decrease.
- The PSP temperature dependence was minimal for the low-enthalpy, short-duration runs on aluminum. An estimated 1% decrease in intensity was associated with increasing coating temperature despite a 15–25 K temperature increase in the flow. This small response of the coating to the thermal changes in the flow is believed to be caused by the

high thermal conductivity and large mass of the test plate compared to the coating.

## References


**Baron A; Danielson D; Gouterman M; Wan J; Callis J; McLachlann B** (1993) Submillisecond response times of oxygen quenched luminescent coatings. Rev Sci Instr 64: 3394–3402

**Borovoy V; Bykov A; Mosharov V; Orlow A; Radchenko V; Phonov S** (1995) Pressure sensitive paint application in a shock wind tunnel. 16th ICIASF Record. 34.1–34.4

**Carroll B; Abbitt J; Lukas E; Morris M** (1996) Step response of pressure sensitive paints. AIAA J 34: 521–526

**Hubner J; Carroll B** (1997) Application of dual sorption theory to pressure-sensitive paints. AIAA J 35: 1790–1792

**Lui T; Campbell B; Burns S; Sullivan J** (1997) Temperature- and pressure-sensitive luminescent paints in aerodynamics. App Mech Rev 50: 227–246

**McLachlan B; Bell J** (1995) Pressure-sensitive paint in aerodynamic testing. Exp Thermal and Fld Sci 10: 470–485

**Mendoza D** (1996) Uncertainty analysis of luminescent pressure sensors. Ph.D. thesis, University of California, Mechanical Engineering Department

**Morris M; Donovan J; Kegelmman J; Schwab S; Levy R; Crites R** (1993) Aerodynamic applications of pressure sensitive paint. AIAA J 31: 419–425

**Rogers C** (1985) Permeation of gases and vapours in polymers. Polymer permeability. ed J Comyn pp. 11–73, Amsterdam: Elsevier Applied Science Publishers

**Sajben M** (1993) Uncertainty estimates for pressure sensitive paint measurements. AIAA J 31: 2105–2210

**Schanze K; Carroll B; Korotkevitch S; Morris M** (1997) Concerning the temperature dependence of pressure sensitive paint. AIAA J 35: 306–310

**Vieth W; Howell J; Hsieh J** (1976) Dual sorption theory. J Mem Sci 1: 177–220

**Winslow N; Carroll B; Setzer F** (1996) Frequency response of pressure sensitive paints. Twentyseventh AIAA Fld Dyn Conf Paper 96-1967